Structural properties of Ge-S amorphous networks in relationship with rigidity transitions: An ab initio molecular dynamics study

S. Chakraborty, P. Boolchand, and M. Micoulaut

Phys. Rev. B **96**, 094205 — Published 22 September 2017

DOI: 10.1103/PhysRevB.96.094205

Structural properties of Ge-S amorphous networks in relationship with rigidity transitions: an ab initio molecular dynamics study

S. Chakraborty[1], P. Boolchand[1], M. Micoulaut[2]
[1]*School of Electronics and Computing Systems, College of Engineering and Applied Science, University of Cincinnati Cincinnati, OH 45221-0030, USA and*
[2]*Laboratoire de Physique Théorique de la Matière Condensée, Université Pierre et Marie Curie, 4 Place Jussieu, F-75252 Paris Cedex 05, France*
(Dated: September 5, 2017)

We investigate the amorphous Ge_xS_{100-x} (with $10 \leq x \leq 40$) system from ab initio simulations. Results show a very good agreement with experimental findings from diffraction and the topology of the obtained structural models is further analyzed and compared with the selenide analogue. Differences emerge however from a detailed Molecular Dynamics analysis showing the ring statistics and the homopolar defects to not evolve similarly. The findings are also connected to Rigidity theory which provides a topological approach to decoding the physics of network glasses, and effect of composition and temperature are analyzed.

PACS numbers: 61.43.Fs

I. INTRODUCTION

A topological approach to physics of network glasses was first developed using Rigidity Theory[1,2]. The role of temperature dependent constraints was then introduced[3–5], and more recently, the theory has been extended to systems wherein the octet bonding rule is intrinsically broken using Molecular Dynamic (MD) simulations[6]. The theory has thus evolved into a promising tool making possible to predict topological phases in a variety of glass systems including tellurides[7] and modified oxides[8–11]. In the basic approach two types of mechanical constraints are usually considered; bond-stretching and bond-bending. In 3D, flexible phases form when $n_c < 3$, an isostatically intermediate phase (IP) forms when $n_c \simeq 3$, and a stressed-rigid phase when $n_c > 3$. Here n_c represents the count of constraints per atom. The physical properties of glasses in IPs have attracted widespread attention[12] both at a basic level[13–19] and for applications[20–23] because such networks are stress-free[24], display weak aging[25] as compared to glasses fulfilling $n_c \neq 3$, and can adapt to form compacted networks[26], which are characterized by thermally reversing glass transitions. These phases have now been observed in more than 30 glass systems including heavy metal oxides[27], solid electrolytes[20,28], modified oxides including borates[11], germanates[10] and silicates[8,9].

The case of the Ge-chalcogenides, specially, Ge-S and Ge-Se have been extensively investigated experimentally for several decades in this context[29–35]. The recent experimental report on binary Ge-S glasses[33] on especially homogenized melt glass batch compositions yielding an IP that is strinkingly similar in composition space to the one in Ge-Se binary[34] drew our attention. From the theoretical viewpoint however, Ge-S system has received little attention up to now, albeit recent work has focused on particular compositions (the stoichiometric GeS_2[36–39] and GeS_4[40]). In chalogenides, the major challenge is to reproduce bonding defects that are observed experimentally in diffraction or spectroscopic studies[41–43]. Previous computational schemes and, particularly classical molecular dynamics simulations[44–47] or Reverse Monte Carlo simulations[48–50] have failed in reproducing accurately such features. In addition these chalcogenide glasses and melts display chemical bonding that is partially ionic and partially covalent, while also showing semi-metallic behavior under pressure[51] or with temperature[52]. One has therefore to rely on first-principles molecular dynamics (FPMD), which can account for all the electronic features of chemical bonding. This also allows for the computation of other properties which are inaccessible from classical molecular dynamics such as electronic properties.

In the present work, using FPMD we investigate in a systematic fashion the behaviour of Ge-S glasses, while also exploring new features regarding rigidity that can be directly derived from molecular simulations. In such Group IV chalcogenides, one has a cation (Ge) and an anion (S) that conform to the 8-$\mathcal{N}$ (octet) bonding rule ($\mathcal{N}$ being the number of s and p electrons), leading amongst other things to the formation of a local structure consisting in corner-sharing and edge-sharing $GeS_{4/2}$ tetrahedra. **Results show a very good agreement of the pair correlation function and the structure factor for all compositions, and the corresponding structural models are then analyzed from the viewpoint of topology and rigidity, while also being analyzed in termes of partial pair correlations. Homopolar Ge-Ge bonds form at a composition (25 %) that is lower than the stoichiometric compound (GeS_2, 33 %), and the intermediate range order can be quantified by the ring statistics. It reveals that while 4- (edge-sharing) and 6-fold rings increase with Ge content, one does not observe a threshold behavior close to the stress transition (25 % following Ref.[33]), and one does not obtain a significant increase of 5-fold rings in the Ge-S system. Finally, the calculation of the fraction of bonding constraints permits to quantify accurately the Mauro-Gupta function[3] for the Ge-S system, and to provide new insights into the temperature dependence of topological constraints.**

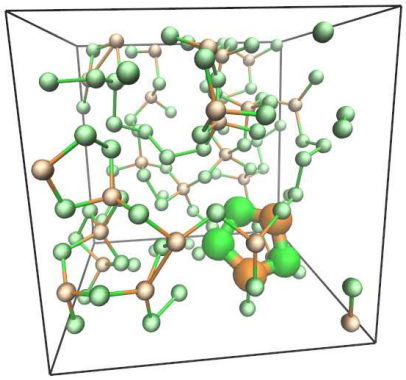

Figure 1: A snapshot of an amorphous GeS_3 showing Ge atoms (orange) cross-linking the sulphur network. A 5-fold ring has been highlighted.

II. NUMERICAL METHODS

Ge-S liquids and glasses have been investigated using Car-Parrinello molecular dynamics (CPMD) simulations[53]. The system contained 120 atoms (Fig. 1), and up to 5 compositions Ge_xS_{100-x} have been simulated in NVT ensemble with cubic cell of sizes allowing one to recover the experimental density of corresponding glasses[33] (e.g. 15.01 Å for $Ge_{10}S_{90}$).

The general methodology is exactly the same as the one used for recent investigations of GeS_2 and GeS_4 glasses[36,40] i.e. we have used density functional theory (DFT) to describe the electronic structure that evolved self-consistently with time. We have adopted a generalized gradient approach (GGA) using the exchange energy obtained by Becke[54] and the correlation energy according to Lee, Yang and Parr (LYP)[55]. The BYLP approach was used because it takes into account valence electron localization effects better than alternative exchange correlation functionals[56,57] as suggested by a better agreement with experiments[41–43] on structure for similar liquids and glasses. In the present investigation, valence electrons have been treated explicitly, in conjunction with norm conserving pseudopotentials of the Trouiller-Martins type to account for core-valence interactions. The wave functions have been expanded at the Γ point of the supercell on a plane-wave basis set having an energy cut-off of 20 Ry which is a standard value for the investigation of chalcogenides[56–61]. A fictitious electron mass of 2000 a.u. was used in the first-principles molecular dynamics (FPMD) approach. The time step for integrating the equations of motion was set at Δt = 0.12 fs. The temperature control was achieved for both ionic and electronic degrees of freedom using Nosé-Hoover thermostats. The initial coordinates of 120 atoms have been constructed by substituting previous configurations of Ge-Se glasses[62]. After a preliminary run at T = 2000 K for a period of 25ps in order to lose the memory of the initial configuration, we have then investigated a certain number of isotherms (1800 K, 1500 K, 1200 K) over 25 ps each, down to 1050 K. At this temperature, four independent configurations separated by 5 ps each have served as starting configurations for a quenching procedure (q=10 K/ps approximatively) and then selected a certain number of target temperatures (800 K, 600 K) prior to a complete recording (70 ps) of glass trajectories at 300 K that have been analyzed. In the forthcoming, most of the structural analysis is performed at 300 K.

The difference in quench rates between the MD simulations (10 K/ps) and the experimental ones (typically 10^3 K/s) deserves some comments. Given this huge difference, the numerical systems have usually all the features of a high-temperature liquid that has been hyperquenched into a local energy minimum (an inherent structure[63]) that does not necessarily reflect the true glassy state given the small time interval (70-100 ps) allowed for relaxation. The four independent quenches are precisely used to partaily circumvent this problem, i.e. by averaging over four independent local minima of the potential energy landscape, one might have a good representation of a potentially more realistic glass structure, the number of independent quenches being limited by computational cost. There are, certainly structural variations and some of these aspects are discussed below.

It should also be stressed that typical cooling rates involved in MD simulations (10^9-10^{13} K/s) are compatible with a general scaling law that applies for size dependent cooling rates. It has been, established, indeed, that q is proportionnal to the volume V over area A ratio of the sample[64], in the case where the mechanism of heat transfer during quench is convection. This scaling law is actually fulfilled for a variety of glass-forming liquids with sizes ranging between 10^{-3} mm[65] and 2 mm[66], the former being compatible with values found for the production of amorphous water[67]. An extrapolation of the obtained scaling law q(V/A) to sizes typical of those involved in the present simulated systems (10-20 Å) is actually compatible with the lower limit of typical MD cooling rates (10^9 K/s).

III. RESULTS

A. Reciprocal space

In order to validate the simulated structural models, we first concentrate on results in reciprocal space that can be directly compared to measurements from diffraction for Ge-S glasses[68–70] (Fig. 2).

Fig. 2 shows the results of the present investigated Ge-S system. First, it is important to emphasize that a very good agreement of the calculated interference function $I(k)$=k[$S(k)$-1] is found when compared to the experimental counterpart. Note that this function $I(k) = k[S(k) - 1]$ blows up the oscillations found at higher k value, which are

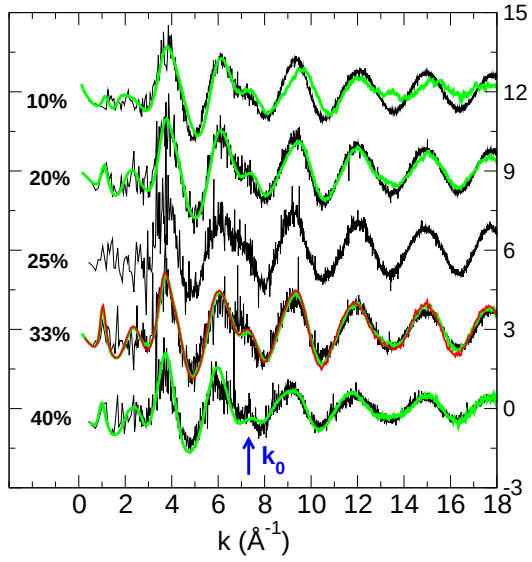

Figure 2: Simulated interference function $k[S(k)-1]$ (black curves) in 300 K Ge-S glasses. The results are directly compared with measured structure factors (colored curves) from neutron diffraction: $Ge_{10}S_{90}$[68], $Ge_{20}S_{80}$[68], $Ge_{33}S_{67}$ (green[68,69] and red[70]), $Ge_{40}S_{60}$[69]. The shoulder peak at $k_0 \simeq$7.5Å is signaled.

damped in the simple $S(k)$ function. This permits to better quantify the degree of agreement between theory and experiments, and, particularly for $k >$8 Å^{-1}. In fact, the present simulations on Ge-S reproduce all typical features over the entire range of wavevectors k and for all compositions. The first sharp diffraction peak (FSDP) is found at $k \simeq 1$ Å^{-1} similarly to experiments[68–70] for compositions larger than 20 % Ge. The simulated first principal peak (PP1) at $\simeq$ 3.5 Å^{-1} and second principal peak (PP2) at $\simeq$6 Å^{-1} are also very well described ; the position, the width and the intensity of the peaks for all considered compositions are excellently reproduced. Similarly, $I(k)$ permits one to detect also a very good agreement in the high wavector region ($k >$10-18 Å^{-1}), and this provides confidence that real space properties at short distance r ($r \propto 1/k$) should be also reasonably well reproduced. However, it should noted that a slight shift in wave-vector is obtained for the lowest Ge-S composition and $k >$ 12 Å, and this may arise from a partial crystallization of the experimental glass sample[68], **as detected experimentally**. The reproduction of the structure factor in such complex glasses (e.g. GeS_2) has been found to moderately depend on the numerical cooling rate[38], the only limiting feature being the correct reproduction of the amplitude of the FSDP. The latter has been found to be strongly dependent on the DFT scheme, and a continuous improvement for the exchange-correlation functional, incorporation of the generalized gradient approximation[75], better account for the semi-conducting nature of the material[56], has led to the identification of the correct electronic scheme, able to reproduce the salient structural features of Ge-S glasses[36,37,39,40].

When investigated as a function of Ge content, we find that a shoulder peak exists at $k_0 \simeq$ 7.5 Å for low content (arrow in Fig. 2), which is also present in experiments. This peak separates from the second principal peak (PP2) only for x=40 %. It is, therefore, believed that structural correlations at the corresponding length $7.7/k_0 \simeq$1 Å will be substantially altered once the glasses have a larger amount of Ge-Ge bonds. An inspection of the corresponding Faber-Ziman structure factors (not shown) $S_{GeGe}(k)$ indicates, indeed, that contributions to the peak at $k = k_0$ mostly arise from such correlations, and also from Ge-Se. In addition, we find that the amplitude of the oscillations in $I(k)$ decrease at high Ge content, and the intensity of the peak at e.g. k_1=12 Å is substantially reduced, i.e. one finds $I(k_1)$=0.75 and 1.35 at $Ge_{40}S_{60}$ and $Ge_{33}S_{67}$, respectively.

B. Real space

The accuracy of the present models can be compared to experiments in real space as well. When investigated as a function of Ge content (Figure 3), one obtained a computed total pair correlation function $g(r)$ for the Ge_xS_{1-x} glasses which is, again, in **good** agreement with available measurements from the literature[68–70]. In fact, for e.g. GeS_2 (Fig. 3) all the features of the pair correlation function are reproduced with **a great accuracy**: main peak at 2.24 Å (experimentally 2.21 Å[70] or 2.24 Å[69]) and a small secondary peak (2.93 Å) whose position and intensity (2.92 Å[70] and 2.94 Å[69]) are found to be close to experimental findings. The third principal peak has its position slightly overestimated (3.65 Å against 3.45 Å[69,70]) and its intensity underestimated with respect to the experimental findings. In GeS_2, one furthermore notices that a fourth shallow peak (5.41 Å) is also rather well reproduced, and all these obtained features are rather systematic for the other compositions, especially when a direct comparison with experiments is avalailable as for $Ge_{10}S_{90}$[68], **$Ge_{20}S_{80}$**[40] and $Ge_{40}S_{60}$[69].

The position of the Ge-S bond length is of about 2.22 Å, i.e. shorter than the one found[42,62] for Ge-Se (2.36 Å). As a result, the large intensity of the first peak of the partial $g_{GeS}(r)$ (Fig. 4) this time does not overwhelms other contributions arising from Ge-Ge correlations[70]. Consequently, the peak associated with the latter can be detected at short distances (2.24 Å for GeS_2) in the total correlation function $g(r)$ and arises from the edge-sharing $GeS_{4/2}$ tetrahedra. Other typical correlating distances between the (Ge,S) species can be detected as a function of Ge content (Fig. 4), i.e. the partial $g_{GeGe}(r)$ reveals three major components made of i) a homopolar distance Ge-Ge (e.g. 2.46 Å in GeS_2) found at high Ge content and which give rise to a so-called ethane-like unit[76], ii) a secondary peak (e.g. at 2.92 Å in $Ge_{20}S_{80}$) associated with the edge-sharing tetrahedra, and iii) a main peak corresponding to corner-sharing (CS) tetrahedra. For the Ge-Se system, these features have been unambiguously identified from the analysis of the full partial resolution using isotopic substitution in neutron diffraction[42]. The difference between the two systems is mostly detectable in the height of the intensity associated with the ES peak, and indicates that the Ge-S binary seems to have an increased tendency to form such a ring struc-

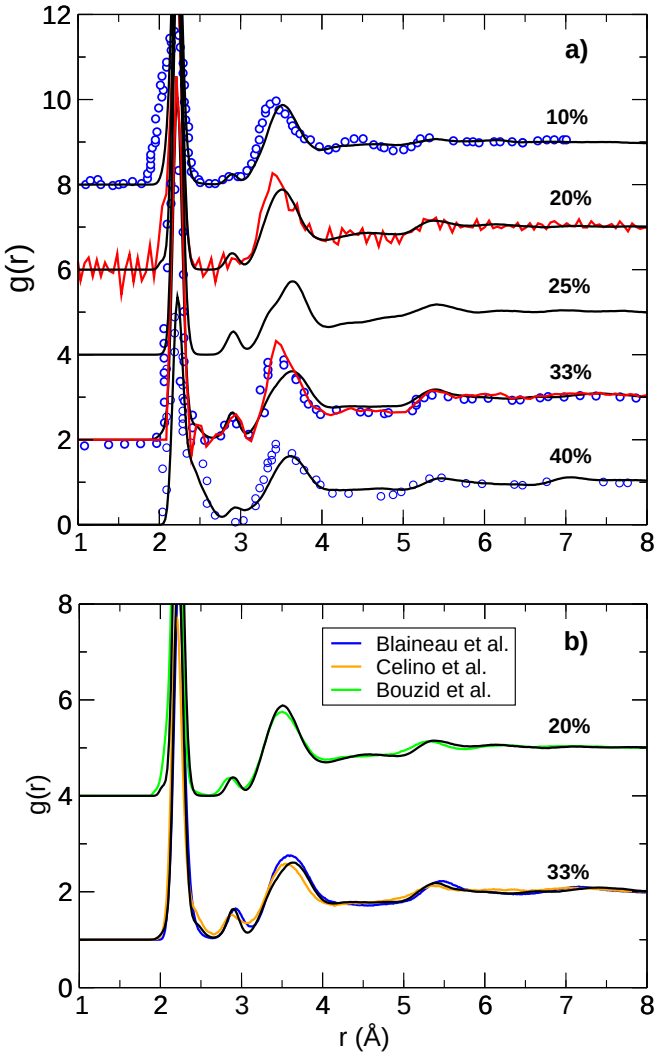

Figure 3: a) Calculated total pair correlation function $g(r)$ in **amorphous** Ge-S (300 K) glasses (black lines) at 300 K, compared to experimental measurements from neutron diffraction: $Ge_{10}S_{90}$[68], **$Ge_{20}S_{80}$ (red curve,[40])**, $Ge_{33}S_{67}$ (circles[68,69] and red curve[70]), $Ge_{40}S_{60}$[69]. b) Comparison of the present simulated GeS_2 (33%) and GeS_4 (20%) with previous simulations from Blaineau et al.[38,39], Celino et al.[36] and Bouzid et al.[40].

ture, at least in Ge-rich glasses, as already revealed from the Raman analysis[33]. In addition, we note that the homopolar Ge-Ge bonds appear only for $Ge_{33}S_{67}$ (Fig. 4a), and this contrasts with the findings of the Ge-Se glasses which already exhibited[62] this corresponding typical prepeak at $Ge_{25}Se_{75}$ (red curves in $g_{GeGe}(r)$ in

The main feature of the pair distribution function $g_{GeS}(r)$ consists of an intense peak that has a large gap with the secondary contributions, and this first peak corresponds to Ge-S distance defining the tetrahedra. The distance, furthermore, satisfies d_{Ge-S}=$\sqrt{3/8}d_{S-S}$ with d_{S-S} being the edge length of the tetrahedra (i.e. the principal peak of $g_{SS}(r)$), and we find that d_{Ge-S}/d_{S-S}=0.60±0.02 and one has 0.61 for a perfect tetrahedron. With increasing Ge content, it is seen that

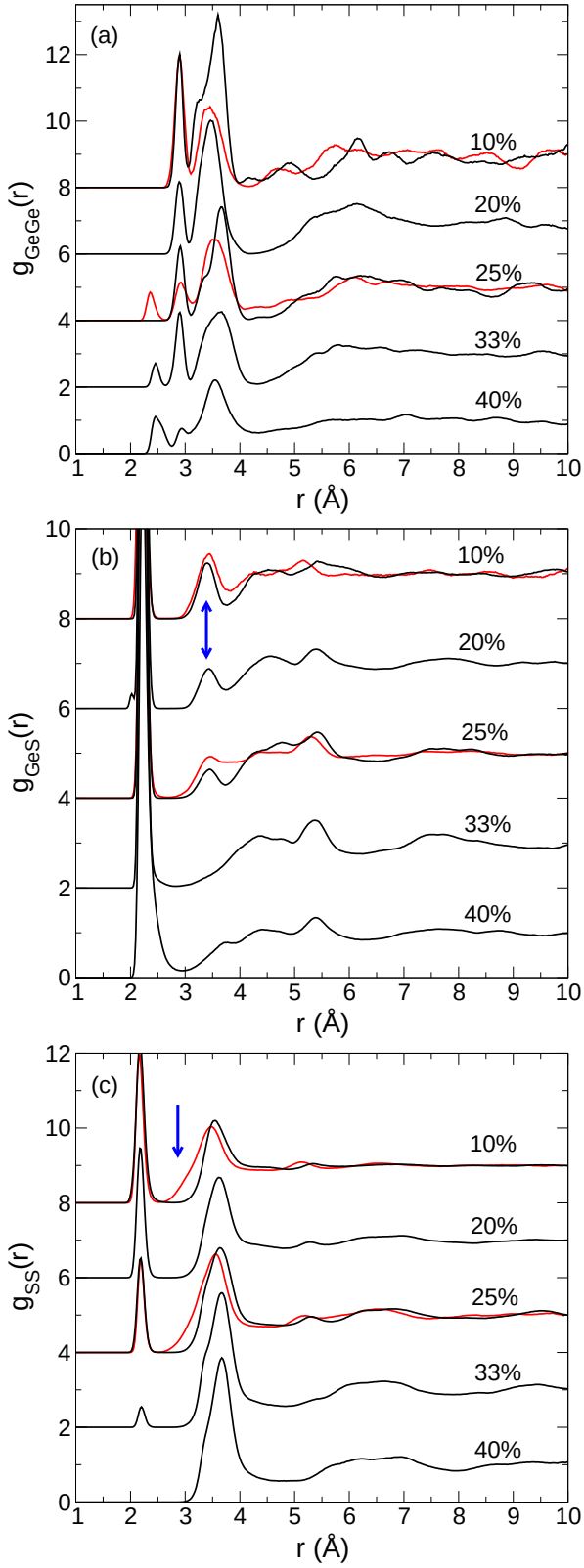

Figure 4: (Color online) Computed pair distribution functions $g_{ij}(r)$ (i,j=Ge,S) as a function of composition x in Ge_xS_{1-x} glasses (300 K). The red curves are results for Ge-Se glasses[62] and serve for comparison. They have been rescaled in distance in order to match the sulphide related functions (see also Fig. 6). The blue arrows indicate structural features discussed below.

the secondary peak (arrows in Fig. 4b) found at ≃3.44 Å low Ge content (e.g. $Ge_{10}S_{90}$) tends to decrease in amplitu as x is increased, and has completely vanished at $x \geq 33$ The origin of this peak[62] can be associated with i) typical d tances involved between a cross-linking Ge atom and a s phur atom being part of a distinct chain, and ii) the seco nearest neighbor distance associated with $GeS_{4/2}$-S-S cor lations along the same sulphur chain. As the chain-like stru ture disappears with increasing Ge content, it becomes harc to find such typical correlating distances and the amplitude the corresponding peak in $g_{GeS}(r)$ decreases to finally vani for $x > 25$ %.

C. Comparison with previous simulations

As stated previously, a certain number of simulatio on select compositions of the Ge-S binary have alrea been reported in the literature, the system size being t only difference (from 96 to 480 atoms, depending on t composition). Figure 3b) reproduces such previous sim lations g-GeS_2[36,38,39] and GeS_4[40]. It should be remark that the total pair correlation function is almost identi for both presented compositions. However, while alm all simulations are relying on an identical DFT scheme, it is important to emphasize that some of them[38,39] use a non-self-consistent DFT together with a local density approximation (LDA) and such approximate schemes lead to a smaller amount of homopolar bonds and threefold coordinated sulfur atoms[40], the only other difference being an increased sharpness for the first peak of $g(r)$ which is the signature of a more structured network.

On the overall, it is seen that differences are minimal, and even potential effects[71] of system sizes (120 atoms for the present simulation, 480 in ref.[40], 96 atoms in ref.[38]) are barely visible.

D. Defects and thermal history

Figure 5 shows the effect of thermal history on the structure of $Ge_{40}S_{60}$. Here is represented the Ge-Ge correlations in $g_{GeGe}(r)$ of the four quenched amorphous samples obtained after a melt quench from an equilibrated temperature of 1050 K (see Methods), and corresponding energies are provided in order to quantify the relationship of the underlying energy landscape with structural properties. It is important to emphasize that corresponding structural correlations for Ge-S and S-S (not shown) are weakly impacted by the thermal history so that the four corresponding partial pair correlation functions almost overlap onto each other. This simply indicates that the base tetrahedra (Ge-S distances at 2.22 Å and tetrahedral edges, S-S distances, at 3.55 Å) act as building blocks for the corresponding structure and are weakly altered by the quench. This situation contrasts with the one encountered for Ge-Ge correlations which exhibit some more significant differences. Results indicate that the structure with the lowest

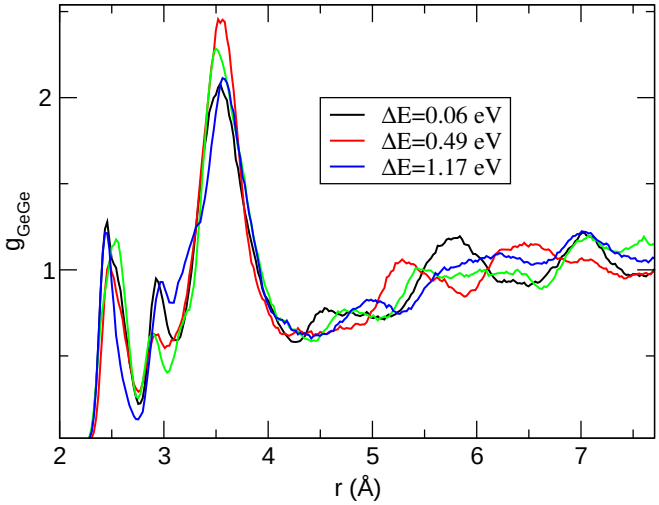

Figure 5: (Color online) Partial pair correlation function $g_{GeGe}(r)$ of $Ge_{40}S_{60}$ for the four independent quenches. The lowest energy minimum corresponds to the green curve (E=-26.415 keV) and energy differences are provided.

energy (or lowest fictive temperature, green curve) contains the smallest ring fraction (secondary peak at 2.8 Å) given the weakest amplitude, a qualitative result that has been also found in other glassy materials including silica[72]. It is also seen that the fraction of homopolar defects is influenced by the energy of the system reached after the quench, as is the Ge-Ge homopolar distance, the sample with the lowest energy having also a slightly longer homopolar distance (2.54 Å vs 2.45 Å) and a reduced Ge-Ge correlation distance for the ES motif (2.89 Åvs 2.95 Å). It would certainly be of interest to relate in more detail characteristics of the energy landscape and the energy of inherent structures with structural properties[73,74] of the obtained glassy materials but such a study is unfortunately beyond the possibilities of DFT based methods given the limitation in size and equilibration time. One is, therefore, left at a rather qualitative albeit insightful level of description.

IV. DISCUSSION

Now that the obtained structural models have been validated and successfully compared to experiments, we concentrate on the topology of such Ge-S networks and relate results with aspects of rigidity, and compare with the parent Ge-Se system.

A. Coordination numbers

In Table I, we report the partial pair coordinations n_{ij} calculated from the partial pair correlation functions (Fig. 4). One obtains a decrease of the partial coordination numbers n_{GeS} with increasing Ge content once homopolar Ge-Ge have

Table I: Calculated pair coordination numbers n_{ij}, coordination numbers n_i and mean coordination number $\bar{r}$ in Ge-S and Ge-Se[62] glasses. The cut-off distances for the calculation of the coordination numbers have been taken at the minimum of each pair distribution functions (r_m=2.6-2.9 Å).

	n_{GeGe}	n_{GeX}	n_{XX}	n_{Ge}	n_X	$\bar{r}$
$Ge_{10}S_{90}$	-	4.00	1.56	4.00	2.00	2.20
$Ge_{10}Se_{90}$[62]	-	4.01	1.56	4.01	2.00	2.20
$Ge_{20}S_{80}$	-	3.96	1.00	3.96	1.99	2.38
$Ge_{20}Se_{80}$[62]	-	3.92	1.00	4.01	2.00	2.40
$Ge_{25}S_{75}$	-	3.99	0.67	3.99	2.00	2.50
$Ge_{25}Se_{75}$[62]	0.13	3.87	0.71	4.01	2.00	2.50
$Ge_{33}S_{67}$	0.10	3.85	0.10	3.95	2.03	2.67
$Ge_{33}Se_{67}$[62]	0.25	3.55	0.30	3.80	2.08	2.64
$Ge_{40}S_{60}$	0.37	3.24	-	3.57	2.16	2.72
$Ge_{40}Se_{60}$[77]	0.52	3.21	0.01	3.73	2.15	2.78

emerged for $x \geq 33\%$. On the other hand, n_{SS} decreases with composition x as indicated from the decrease of the amplitude of the homopolar distance in $g_{SS}(r)$. These trends are furthemore found to be very close to those determined for Ge-Se glasses[62,77].

Corresponding total coordination numbers can then be calculated (Table I) using

$$n_i = n_{ii} + \sum_{i \neq j} n_{ij}, \quad (1)$$

and e.g. $(1\text{-}x)n_{SGe} = x n_{GeS}$. Results show a nearly perfect agreement with what can be expected from 8-$\mathcal{N}$ rule, at least for compositions at $x < 40\%$. One finds, indeed, that Ge atoms have a coordination number close to n_{Ge}=4, whereas sulphur atoms have $n_S \simeq 2$. For the composition $Ge_{40}S_{60}$, due to an important fraction of Ge-Ge bonds and to coordination defects, n_{Ge} reduces to 3.57 (3.73 in the corresponding selenide[77]), and n_S slightly increases. An investigation of the population of coordination numbers n^i_{Ge} (with i=3,4,5) shows, indeed, that while Ge-S glasses with $x < 33\%$ have n^4_{Ge}=100%, once the Ge content is larger, three and five-fold Ge emerge which leads to a global decrease to n_{Ge}=3.57. Similarly, an increased fraction of three-fold sulphur is obtained for this Ge-rich composition, and this also contributes to the growth of n_S.

B. S-S and Se-Se correlations contrasted

For the chalcogen-chalcogen correlations, the gap between the first and second principal peaks is actually found to be somewhat larger when the partials $g_{SS}(r)$ and $g_{SeSe}(r)$ are being compared, indicating a less structure for the selenide glass between the first and the second shell of neighbours. This can

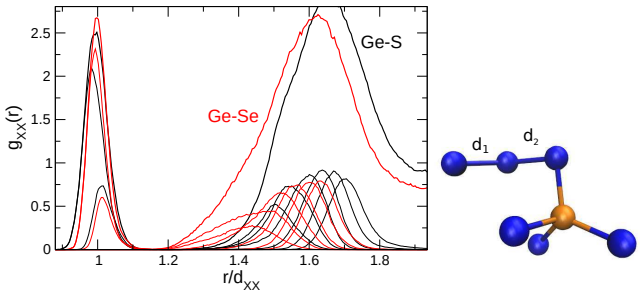

Figure 6: (Color online) Left: Calculated neighbor distributions in $Ge_{25}S_{75}$ (black lines) and $Ge_{25}Se_{75}$ (red curves, adapted from[62]) as a function of a rescaled distance r/d_{XX} where d_{XX} is the first peak of the partial chalcogen-chalcogen correlation function (2.19 Å and 2.36 Å for S-S and Se-Se, respectively). The thick lines correspond to the partial $g_{SS}(r)$ and $g_{SeSe}(r)$ also displayed in Fig. 4c. Blue bars define the first and second neighbour distances d_1 and d_2 for the Ge-S glasses. Right: A typical fragment of S-rich Ge-S glasses showing the distances d_1 and d_2.

be detected from the tail appearing on the left side of the secondary peak, i.e. at $r \simeq 3$ Å (red curves in Fig. 4c and blue arrow). This tail arises from a more compacted second coordination shell, and, particularly, from the 3- and 4th selenium neighbors (Fig. 6, left). In order to contrast both systems, g_{SS} of Fig. 4c can be rescaled by the homopolar bond distance d_{SS} corresponding to the principal (first or homopolar) peak of the function $g_{SS}(r)$. **A similar procedure can be realized for Ge-Se glasses to lead figure 6 which represents now such a rescaled chalcogen-chalcogen pair correlation function** $g_{XX}(r)$ **(X=S,Se).** Corresponding 3 and 4-neighbour distributions are found at larger r/d_{XX} distances in the sulphur glasses, i.e. $r = 1.4 d_{S-S}$ as compared to the selenium system ($r = 1.2 d_{Se-Se}$). On might argue that this can be an effect due to compaction but it is worth emphasizing that Ge-Se displays a smaller density[32] as compared to Ge-S[33]. It can be also detected that the amplitude and the average position (d_1 and d_2, blue bars in Fig. 6) of the two first neighbour distributions contributing to the prepeak in $g_{SS}(r)$ are not equal, and these also turn out to be composition dependent with the amplitude of the peak at d_1 continuously decreasing with Ge content for $x < 33\%$. In fact, the second distribution at d_2 is identified with a homopolar distance close to a $GeS_{4/2}$ tetrahedron (Fig. 6, right), and is on average slightly shorter (2.15 Å) when compared to the one having no Ge tetrahedra in its vicinity (d_1=2.22 Å for $Ge_{20}S_{80}$). This might result from an increased Coulombic interaction due to the Ge^{4+} centers.

C. Homopolar bondings

Next, we calculate from the trajectories the fraction of homopolar bonds in the Ge-S glasses and compare them with previous results on Ge-Se[62] and bond statistics obtained from Reverse Monte Carlo modelling of Ge-Te[78]. Figure 7 shows the evolution of Ge-Ge and chalcogen-chalcogen (S-S, Se-Se, Te-Te) bonds with increasing Ge content.

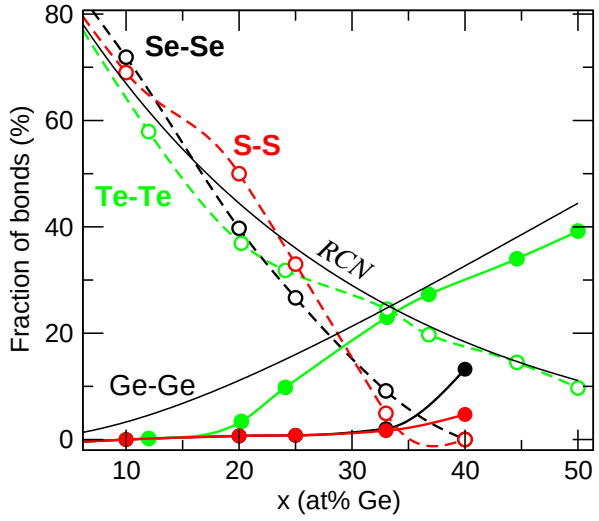

Figure 7: (Color online) Calculated fraction of Ge-Ge (filled symbols, solid line) and chalcogen-chalcogen (open symbols, broken lines) homopolar bonds in Ge-S (red), Ge-Se[62] (black) and Ge-Te[78] (green) glasses as a function of Ge content. The cutoff has been chosen at the minimum of each pair correlation function. The thin lines represent the RCN model of equs. (2)-(3).

For all, a decrease of the chalcogen-chalcogen bonds is obtained, accompanied by a growth of Ge-Ge bonds, the results exhibiting clear differences when the different families of binary chalcogenides are being directly compared. At low Ge composition (x <20 %), all Ge-based chalcogenides including Ge-Te[78] behave similarly, and this arises from the fact that $GeTe_{4/2}$ motifs are dominated by a tetrahedral geometry[6] for x <20 % so that the same short range order is encountered for all. At larger Ge content however (x >20 %), the decrease of Te-Te bond population behaves differently, and deviates from the S-S and Se-Se curves, and this arises from the increasing presence of Ge defect octahedra which increases the possibility of homopolar bonding in the structure. The presence of such octahedra and the existence of the crystalline polymorph GeTe[79] ($GeTe_2$ does not exist) contrasts with lighter chalcogenides, and modifies the tendency towards local chemical order (100 % heteropolar) that prevails in the 25<x<33 % region for Ge-S and Ge-Se glasses. Also, in Ge-Te the remaining Ge tetrahedra are found to involve predominantly Ge-Ge bonds[80] which also leads to additional chemical disorder with respect to what would be expected from the nominal composition.

The weaker amplitude of the pre-peak in $g_{GeGe}(r)$ in Ge-S glasses (Fig. 4c) leads to a lower population of Ge-Ge bonds, and only 4.73 % of Ge-Ge bonds are found in $Ge_{40}S_{60}$, a result that contrasts with the behaviour of Ge-Se (13.2 % in $Ge_{40}Se_{60}$). Also, the combined trends of Ge-Ge and (S-S,Se-Se) does not lead to a minimum in the heteropolar bond statistics as detected for Ge-Te[78] or in other chalcogenides[81]. This difference in behaviour can be roughly explained by the fact that Ge-Te glasses follow bond statistics that are close to the random covalent network (RCN) picture for which the populations are given by:

$$p^{RCN}_{GeGe} = \frac{16x^2}{\bar{r}^2} \tag{2}$$

$$p^{RCN}_{XX} = \frac{4(1-x)^2}{\bar{r}^2} \tag{3}$$

with $X = (S, Se)$ and which assumes a continuous increase of Ge-Ge bonds with Ge content (thin black lines in Fig. 7). However, such a distribution leads to a maximum for the heteropolar distribution p^{RCN}_{GeX} at x=1/3, in contrast with numerical findings[78,81] which exhibit an opposite trend (minimum in p_{GeX}). On the other hand, at a crude level the distribution for Ge-S (Fig. 7) is found to be closer to a chemical ordered network (CON) picture for which it is assumed that there are no Ge-Ge bonds for x <33 % Ge and no S-S bonds for x >33 % so that $p^{CON}_{XX} \propto$(1-3x). However both FPMD results and neutron diffraction results[42] indicate a small but significant departure from this CON picture because such homopolar defects are present in the glasses at the stoichiometric composition (33.3 %, Fig. 3).

D. Ring statistics

Topological intermediate range order of Ge-S glasses can then be evaluated. We use for this purpose a ring statistics algorithm that is part of the Rigorous Investigation of Networks Generated using Simulation (RINGS) code[82]. We have used a cutoff distance of 2.6 Å, corresponding to the minimum r_m of the pair distribution function (Fig. 3). This algorithm is based on the King[83]-Franzblau[84] shortest path search to find rings containing a maximum of a number of given atoms. **The shortest path is searched starting from two of the nearest neighbors of a given node (atom), and then propagated from neighbour to neighbour.**

Figure 8 shows the ring statistics $R^{(n)}$ for the five compositions of interest in the Ge-S system. These results also recover recent ring statistics on the selected compositions GeS_2[36] and GeS_4[40], and results are found to be similar. It is important to emphasize that all size n of rings are involved in both glass system, i.e. odd or even sized rings. **Also, no restriction is made for purely heteropolar rings (ABAB rings[58]) so that all sorts of rings containing all possible homo- (Ge-Ge and S-S) and heteropolar (Ge-S) based rings are enumerated. The presence of odd- and even sized rings (e.g. GeS_2) is clearly detectable from Fig. 8).** For GeS_2, this situation contrasts with corresponding stoichiometric oxide glasses (SiO_2, GeO_2) which have only heteropolar bonds and whose network structure will contain only even sized rings[86,87]. The difference with oxides arise from the presence of homopolar bonds (Ge-Ge, S-S, Fig. 7) which permit to have closed loops of odd size. The presence of such motifs is, thus, an indication of the presence of homopolar bonds, this indication being of particular crucial importance for the stoichiometric GeS_2 (or $GeSe_2$[62]) compositions. However, such odd-sized rings are

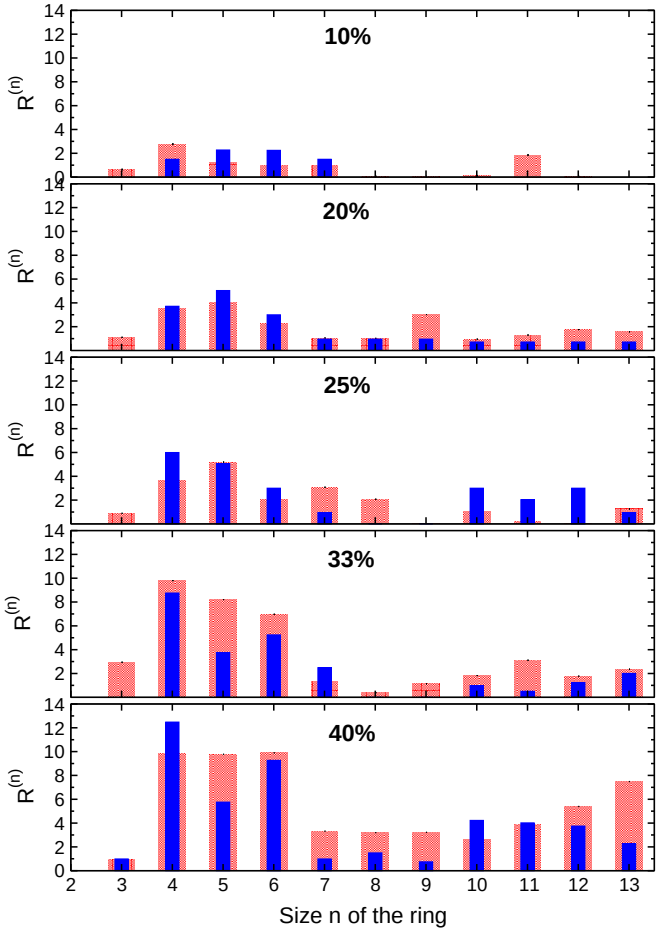

Figure 8: (Color online) Calculated number of rings $R^{(n)}$ in amorphous Ge_xS_{1-x} (blue bars) for different Ge compositions using the RINGS method[82]. Results are compared to the calculated statistics of Ge-Se glasses[62,77] (red bars).

encountered at all compositions covering the S- or Ge- rich domain of the glass-forming region.

In Fig. 8 we, furthermore, find that the increase of Ge content tends to increase the number of possible ring structures. At low Ge content (i.e. 10 %), one finds only a limited number of rings ($R^{(n)}$ <6) due to the chain-like nature of the structure. We do not find any S_8 like rings which are found experimentally at low Ge content[33]. The size of the system (120 atoms) may not be sufficient to detect such ring structures. A recent numerical investigation[40] on GeS_4 on a larger system (480 atoms) has led to similar statistics but this composition probably does not contain any S_8 any more. Classical molecular dynamics simulations[88] performed on larger system sizes (1000 atoms) have shown that the emergence of such S_8 rings is largely driven by relaxation phenomena, and transition states allowing for the conversion of rings into polymeric sulphur chains, and may, therefore, not be available on typical simulation times (ps-ns).

As mentioned above, because the Ge content leads to an overall increased tendency to cross-link the glass network, a global growth of all types of rings[82] is acknowleged (Fig. 8).

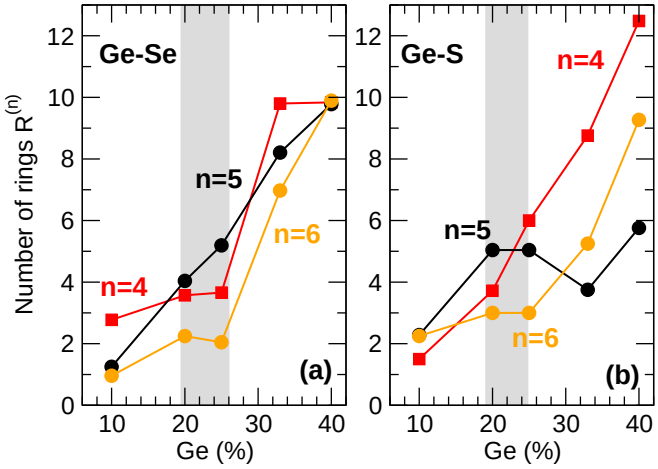

Figure 9: (Color online) Number of small rings $R^{(n)}$ ($3 < n < 8$) in amorphous Ge_xSe_{1-x}[62] (a) and Ge_xS_{1-x} (present work, (b)) as a function of Ge composition x. The grey zone indicates the experimentally determined intermediate phase[30,33]).

The distribution is dominated by two populations, i.e. very small rings (n <7) and larger rings (13> n >9), the former containing either four (ES motifs), five or six atoms. These rings represent the elementary building blocks of the outrigger raft model[89] that has been proposed for $GeSe_2$ and GeS_2, and remains quite popular in the literature. However, it has been shown recently[62] that the calculated rings statistics in $GeSe_2$ does not match the one proposed for this simple structural model. The calculated ring ratio for 4,5 and 6-fold rings is, indeed, 10:8:7, respectively, i.e. quite different from the one of the outrigger raft structure (1:2:2 of Fig. 2 in Ref. 89). The present GeS_2 also supports this conclusion because we find a ratio of about 8:4:5, respectively, also different from the one obtained for $GeSe_2$[62], the latter containing a larger fraction of 5-fold rings. This increased presence of 5-rings essentially arises from a larger fraction of homopolar Ge-Ge bonds present in the structure of Ge-Se which promote the smallest odd rings (Fig. 9). Finally, one recognizes that the outrigger raft model does not contain Ge-Ge bonds while only 5-fold rings ($R^{(5)}$) are assumed to contain homopolar chalcogen-chalcogen bonds. The detail of the analysis of GeS_2 shows that a variety of Ge-Ge, Ge-S and S-S bonding types are present in 5- and 6-fold rings, in contrast with the proposed structure[89].

E. Temperature behaviour of constraints

Using the atomic trajectories obtained from MD, we can now estimate the number of constraints per atom as a function of Ge content and temperature. To calculate n_c, we use recently developed MD-based constraint counting algorithms[5,7], i.e. we estimate the radial and angular excursions between pairs or triplets of atoms, based from the atomic configurations at fixed thermodynamic conditions (x,T). This enumeration is directly inspired by the classical mechanics

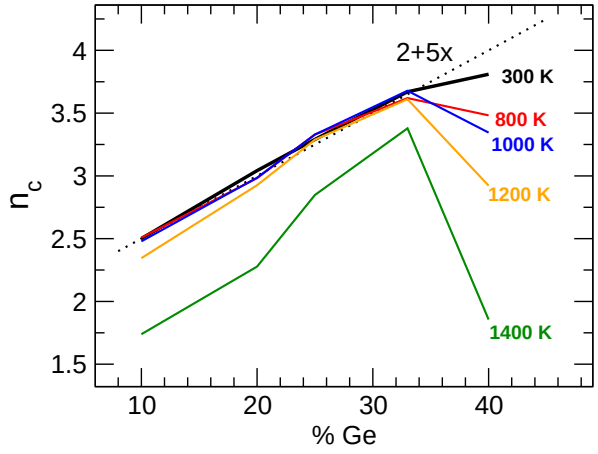

Figure 10: Evolution of the number of constraints n_c for different isotherms as a function of Ge content in Ge-S glasses and liquids. The dotted line is the mean-field estimate n_c=2+5x[1].

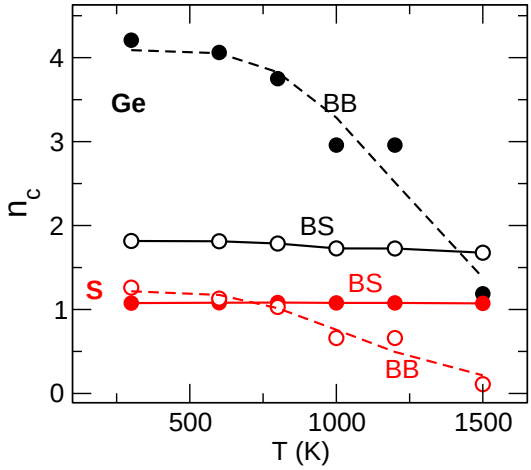

Figure 11: Temperature evolution of the number of constraints in $Ge_{40}S_{60}$ for Ge (black) and S (red). The broken lines are least-squares fit using the Mauro-Gupta form (equ. (4))

view of mechanical constraints associating large/small radial or angular motion with the absence/presence of corresponding bond-stretching (BS) and bond-bending (BB) restoring forces[1,2]. BS constraints can be simply enumerated from the coordination number r of the atoms[5,7,59], and this leads to a contributions of n_c^{BS}=r/2 for the BS constraint. To derive angular (BB) constraints, one follows the angular motion around each individual atom k (k=Ge,S) defined by a set of two neighbors. Over the time trajectory, the corresponding bond angle distribution $P_k(\theta)$ allows defining a mean (the first moment of $P_k(\theta)$) and a standard deviation σ_k (the second moment) that shows a bimodal distribution for the various considered conditions[5,62]. Atoms subject to a rigid bending interaction contribute to the part of the distribution with low σ_k, which corresponds to angles acting as a rigid BB constraint. Averages over the whole simulation box then lead to the mean number of constraints n_c^{BB} per atom. The total number of constraints is then n_c=n_c^{BB}+n_c^{BS} and can be represented as a function of Ge content and temperature (Fig. 10).

First, results point out that the MD based constraint count at low Ge content follows exactly the prediction of a mean-field constraint count[1,2] leading to n_c=2+5x at 300 K **(dotted line in Fig. 10)**. This behaviour is maintained as long as the system remains at low temperature. However, one acknowledges at large Ge content (40 %) a progressive deviation of the calculated n_c with respect to the mean-field result, indicating a softenting of constraints, similarly to the previous study on Ge-Se glasses[62]. The detail of the analysis shows that this reduction of n_c arises from a breakdown of some angular constraints involving the farthest neighbor of a Ge atom, which leads to a decrease of n_c^{BS}.

An increase of the temperature shows that the 40 % composition is highly sensitive to temperature changes, and that all Ge-S compositions start to deviate from the (2+5x) line only at high temperature. The evolution is found to be mostly triggered by the softening of the BB interactions (Fig. 11). In fact, while the number of BS constraints is found to be nearly independent of T (weak coordination change), we find a marked evolution of BB constraints with temperature as n_c^{BB} for Ge atoms decrease from a value that is slightly lower than the mean-field estimate of n_c^{BB}=5 at 300 K to about 1 for 1500 K. Similarly, the S-related number of BB constraints decreases from n_c^{BB}=1 to nearly zero at high temperature, indicating that all S-centred angles have substantially softened. These results actually are partially in agreement with the assumptions made for a temperature-dependent constraint model of network glasses[3]. Here, it was assumed that the Se BB constraint is soft as it induces the breakdown of the medium-range structure with increasing temperature. However, it has been also argued that the Ge angular constraint is by far the strongest constraint due to its sp^3 hybridization of the orbitals. This assumption seems to be contradicted from the present detailed findings given the evolution of n_c^{BB} for germanium atom that soften already at rather low temperature, whereas the BS constraints almost do not vary. Using the Mauro-Gupta form[3] for the prediction of the temperature behaviour of constraints $n_c^i(T)$=$q^i(T)n_c^i(0)$ with i=(BS,BB):

$$q(T) = \left[1 - \exp\left(-\frac{\Delta F^*}{k_B T}\right)\right]^{\nu t_{obs}} \qquad (4)$$

we can establish the associated activation energies ΔF^* of corresponding constraints. Here ν is a vibrational attempt frequency and t_{obs} a typical observation time[90]. We find ΔF^*=0.41(0) eV and 0.32(8) eV for Ge and S BB constraints, respectively, and this permits to determine the onset temperatures T_α of broken constraints via[91]:

$$k_B T_\alpha = \frac{\Delta F^*}{2^{-1/\nu t_{obs}} - 1} \qquad (5)$$

leading to T_α=1316 K and 1109 K for Ge and S BB constraints, respectively. These values are found to differ from those obtained for Ge-Se[3], i.e. it was found T_α >700 K and 218 K for Ge and Se, respectively. It would be interesting to

check if the empirical model built for Ge-Se[3] can be proposed for Ge-S using the presently established parameters.

The other main outcome of the constraint analysis is that changes induced by temperature are small for temperatures lower than 1200 K and for $x \leq 33$ % so that a constraint count at low temperature can hold in liquid and also in the vicinity of the glass transition. These conclusions are consistent with recent results on Ge-Se melts from neutron spin-echo spectroscopy showing that the rigidity concept can be extended from the glass to the liquid[92]. In this work, parameters giving the temperature dependence of the relaxation patterns of binary chalcogen melts have indeed shown to be linearly dependent with the low temperature mean coordination number $\bar{r}$, and thus to follow the count achieved at low temperature. Similarly, relaxational phenomena in Ge-Se using the low temperature constraint approach have also been reported from liquid-state NMR[93].

V. SUMMARY AND CONCLUDING REMARKS

In this article, we have focused on the atomic structure of Ge-S glasses with changing Ge content. These represent archetypal chalcogenide systems that can serve for the experimental validation of flexible to rigid transitions[1,2]. The understanding of their physical and chemical properties in connection with structural and vibrational properties are of great interest given that a certain number of optoelectronic applications of ternary or multicomponent glassy materials use such binary Ge-Se and Ge-S as starting materials.

In order to gain more details into the network structure, we have used recently optimized First Principles Molecular Dynamics (FPMD) simulations to investigate in detail the effect of Ge composition on various properties in the Ge-S system by focusing on five target compositions $Ge_{10}S_{90}$, $Ge_{20}S_{80}$, $Ge_{25}S_{75}$, $Ge_{33}S_{67}$ (GeS_2) and $Ge_{40}S_{60}$. The direct comparison of the calculated pair correlation function $g(r)$ and the structural factor $S(k)$ with results from neutron diffraction shows an agreement of unprecedented accuracy, and provides a validation of the structural models. These can then be used to extract other key features that emerge as the network is progressively cross-linked. The addition of Ge atoms into the base sulphur-rich network leads, indeed, to a continuous growth of 4- and 6-membered rings, whereas 5-fold rings do not seem to increase upon Ge addition. The trends are qualitatively consistent with those determined from the Raman investigation[31,33]. There is a lower tendency in Ge-S to form homopolar Ge-Ge bonds, as compared to Ge-Se, and these occur, indeed, at a composition (33 %) that is lower than in selenides (25 %) and tellurides (20 %).

However, although some structural differences between Ge-Se and Ge-S glasses have emerged from the detailed FPMD investigation, and given that these compositions spanning elastic phases predicted by Rigidity Theory yield almost identical rigidity (20 %) and stress (25 %) transitions[33], one is, ultimately led to believe that local topology and the network connectivity driven by the 8-$\mathcal{N}$ rule determines the location of the IP of these two glass binaries.

PB acknowledges support from NSF grant DMR-08-53957. P.S. Salmon and E. Bychkov are acknowledged for providing their experimental data on diffraction.

[1] J.C. Phillips, J. Non-Cryst. Solids **34**, 153 (1979).
[2] M.F. Thorpe, J. Non-Cryst. Solids **57**, 355 (1983).
[3] P.K. Gupta and J.C. Mauro, J. Chem. Phys. **130**, 094503 (2009).
[4] M. Smedskjaer, J.C. Mauro, R.E. Youngman, C.L. Hogue, M. Potuzak, Y. Yue, J. Phys. Chem. B **115**, 12930 (2011).
[5] M. Bauchy, M. Micoulaut, J. Non-Cryst. Solids **357**, 2530 (2011).
[6] M. Micoulaut, K. Gunasekera, S. Ravindren, P. Boolchand, Phys. Rev. B **90**, 094207 (2014).
[7] M. Micoulaut, C. Otjacques, J-Y. Raty, C. Bichara, Phys. Rev. B **81**, 174206 (2010).
[8] Y. Vaills, T. Qu, M. Micoulaut, F. Chaimbault, P. Boolchand, J. Phys. Condens. Mater. **17**, 4889 (2005).
[9] M. Micoulaut, Am. Mineral. **93**, 1732 (2008).
[10] R. Rompicharla, D.I. Novita, P. Chen, P. Boolchand, M. Micoulaut, W. Huff, J. Phys. Cond. Matt. **20**, 202101 (2008).
[11] S. Vignarooban, P. Boolchand, M. Malki, M. Micoulaut, EPL **108**, 56001-(2014).
[12] *Rigidity and Boolchand Intermediate Phases in Nanomaterials*, M. Micoulaut, M. Popescu Eds., INOE Publishing House, Bucarest, 2009.
[13] M.F. Thorpe, D.J. Jacobs, M.V. Chubynsky, J.C. Phillips, J. Non-Cryst. Solids **266-269**, 859 (2000).
[14] J. Barré, A.R. Bishop, T. Lookman, A. Saxena, Phys. Rev. Lett. **94**, 208701 (2005).
[15] M. Micoulaut, J.C. Phillips, Phys. Rev. B **67**, 104204 (2003).
[16] M.V. Chubynsky, M.A. Brière, N. Mousseau, Phys. Rev. E **74**, 016116 (2006).
[17] K. Trachenko, M.T. Dove, V. Brazhkin, F.S. El'kin, Phys. Rev. Lett. **93**, 135502 (2004).
[18] F. Inam, G. Chen, D.N. Tafen, D.A. Drabold, Phys. Stat. Sol. B **246**, 1849 (2009).
[19] L. Yan, M. Wyart, Phys. Rev. Lett. **113**, 215504 (2014).
[20] D. Novita, P. Boolchand, M. Malki, M. Micoulaut, Phys. Rev. Lett. **98**, 195501 (2007).
[21] *Rigidity and Boolchand Intermediate Phases in Nanomaterials*, edited by M. Micoulaut and M. Popescu, INOE Publishing House, Bucarest, 2009.
[22] D. J. Jacobs, A. J. Rader, L. A. Kuhn, and M. F. Thorpe, Proteins **44**, 150 (2001).
[23] B.J. Madhu, H.S. Jayanna, and S. Asokan, Eur. Phys. J. B, **71**, 21 (2009).
[24] F. Wang, S. Mamedov, P. Boolchand, B. Goodman, M. Chandrasekhar, Phys. Rev. B **71**, 174201 (2005).
[25] S. Chakravarty, D.G. Georgiev, P. Boolchand, M. Micoulaut, J. Phys. Condens. Mater. **17**, L7 (2005).
[26] C. Bourgel, M. Micoulaut, M. Malki, P. Simon, Phys. Rev. B **79**, 024201 (2009).
[27] S. Chakraborty, P. Boolchand, M. Malki, M. Micoulaut, J. Chem. Phys. **140**, 014503 (2014)
[28] M. Micoulaut, M. Malki, D.I. Novita, P. Boolchand, Phys. Rev. B

80, 184205 (2009).
[29] S. Bhosle, K. Gunasekera, P. Boolchand, M. Micoulaut, Int. J. Appl. Glass Sience **3**, 189 (2012).
[30] S. Bhosle, P. Boolchand, M. Micoulaut, C. Massobrio, Solid State Comm. **151**, 1851 (2011).
[31] S. Chakraborty, P. Boolchand, M. Malki, M. Micoulaut, J. Chem. Phys. **140**, 014503 (2014)
[32] R. Bagheria, K. Gunasekera, P. Boolchand, M. Micoulaut, Phys. Status Solidi **251**, 1322 (2014)
[33] S. Chakraborty, P. Boolchand, J. Phys. Chem B **118**, 2249 (2014).
[34] S. Bhosle, K. Gunasekera, P. Boolchand, M. Micoulaut, Int. J. Appl. Glass Sience **3**, 205 (2012).
[35] K. Gunasekara, S. Bhosle, P. Boolchand, M. Micoulaut, J. Chem. Phys. **139**, 164511 (2013)
[36] M. Celino, S. Le Roux, G. Ori, B. Coasne, A. Bouzid, M. Boero, C. Massobrio, Phys. Rev. B **88**, 174201 (2013).
[37] S. Le Roux, P. Jund, Comp. Mater. Sci. **49**, 70 (2010).
[38] S. Blaineau, S. Le Roux, P. Jund, J. Phys. Cond. Matt. **19**, 455207 (2007).
[39] S. Blaineau, P. Jund, D. Drabold, Phys. Rev. B **67**, 094204.
[40] A. Bouzid, S. Le Roux, G. Ori, M. Boero, C. Massobrio, J. CHem. Phys. **143**, 034504 (2015).
[41] I.T. Penfold, P.S. Salmon, Phys. Rev. Lett. **67**, 97 (1991).
[42] I. Petri, P.S. Salmon, Phys. Chem. Glasses **43C**, 185 (2002).
[43] P.S. Salmon, J. Non-Cryst. Solids **353**, 2959 (2007).
[44] P. Vashishta, R.K. Kalia, G.A. Antonio, I. Ebbsjö, Phys. Rev. Lett. **62**, 1651 (1989).
[45] P. Vashishta, R.K. Kalia, G.A. Antonio, J.P. Rino, H. Iyetomi, I. Ebbsjö, Solid St. Ionics **40-41**, 175 (1990).
[46] J.C. Mauro, A.K. Varshneya, J. Am. Ceram. Soc. **89**, 1091 (2005).
[47] M. Wilson, B.K. Sharma, C. Massobrio, J. Chem. Phys. **128**, 244505 (2008).
[48] K.D. Machado, J.C. de Lima, C.E.M. Campos, A.A.M. Gasperini, S.M. de Souza, C.E. Maurmann, T.A. Grandi, P.S. Pizani, Solid St. Comm. **133**, 411 (2005).
[49] A.H. Moharram, A.M. Abdel-Basset, Physica B **405**, 4240 (2010).
[50] K.D. Machado, J.C. de Lima, C.E.M. Campos, T.A. Grandi, P.S. Pizani, J. Chem. Phys. **120**, 329 (2004).
[51] M. Duranduru, D.A. Drabold, Phys. Rev. B **65**, 104208 (2002).
[52] A.A. Andreev, B.T. Melekh, T. Turganov, Sov. Phys. Solid State **18**, 141 (1976).
[53] R. Car and M. Parrinello, Phys. Rev. Lett. **55**, 2471 (1985).
[54] A. D. Becke, Phys. Rev. A **38**, 3098 (1988).
[55] C. Lee, W. Yang and R.G. Parr, Phys. Rev. B **37**, 785 (1988).
[56] M. Micoulaut, R. Vuilleumier, C. Massobrio, Phys. Rev. B **79**, 214204 (2009).
[57] C. Massobrio, M. Micoulaut, P.S. Salmon, Solid State Sci. **12**, 199 (2010).
[58] J. Kalikka, J. Akola, J. Larrucea, R.O. Jones, Phys. Rev. B **86**, 144113 (2012).
[59] M. Bauchy, M. Micoulaut, M. Celino, M. Boero, S. Le Roux, C. Massobrio , Phys. Rev. B **83**, 054201 (2011).
[60] M. Micoulaut, M.-V. Coulet, A. Piarristeguy, M. R. Johnson, G. J. Cuello,C. Bichara,J.-Y. Raty, H. Flores-Ruiz, A. Pradel, Phys. Rev. B **89**, 174205 (2014)
[61] M. Kibalchenko, J.R. Yates, C. Massobrio, A. Pasquarello, Phys. Rev. B **82**, 020202 (2010).
[62] M. Micoulaut, A. Kachmar, M. Bauchy, S. Le Roux, C. Massobrio, M. Boero, Phys. Rev. B **88**, 054203 (2013).
[63] P.G. De Benedetti, F.H. Stillinger, Nature **410**, 259 (2001).
[64] J.A.N. Zasadzinski, J. Micros. **150**, 137 (1988).
[65] H. PLattner, L. Bachmann, Int. Rev. Cytol. **79**, 237 (1982).
[66] B. Luyet, F. Gonzalez, Ref. Eng. **59**, 1191 (1951).
[67] S. N. Bhat, A. Sharma and S. V. Bhat, Phys. Rev. Lett. **95**, 235702 (2005).
[68] E. Bychkov, M. Miloshova, D.L. Price, C.J. Benmore, A. Lorriaux, J. Non-Cryst. Solids **352**, 63 (2006)
[69] A. Bytchkov, C.J. Cuello, S. Kohara, C.J. Benmore, D.L. Price, E. Bychkov, Phys. Chem. Chem. Phys. **15**, 8487 (2013).
[70] I. Petri, P.S. Salmon, J. Non-Cryst. Solids **293**, 169 (2001); A. Zeidler, W.E. Drewitt, P.S. Salmon, A.C. Barnes, W.A. Crichton, S. Klotz, H. E. Fischer, C.J. Benmore, S. Ramos, A.C. Hannon, J. Phys. Cond. Matt. **21**, 474217 (2006).
[71] M. Micoulaut, S. Le Roux, C. Massobrio, J. Chem. Phys. **136**, 224504 (2012).
[72] C. Mikkelsen, Jr. and F. L. Galeener, J. Non-Cryst. Solids **37**, 71 (1980).
[73] D.J. Lacks, M.J. Osborne, Phys. Rev. Lett. **93**, 255501 (2004).
[74] Y. Fan, T. Iwashita, T. Egami, Nature Comm. **8**, 15417 (2017).
[75] C. Massobrio, A. Pasquarello, and R. Car, J. Am. Chem. Soc. **121**, 2943 (1999).
[76] S. Mamedov, D.G. Georgiev, T. Qu, P. Boolchand, J. Phys. Cond. Matt. **15**, S2397 (2003).
[77] S. Le Roux, A. Bouzid, M. Boero, C. Massobrio, Phys. Rev. B **86**, 224201 (2012)
[78] A. Piarristeguy, M. Micoulaut, R. Escalier, P. Jovari, I. Kaban, J. van Eijk, J. Luckas, S. Ravindren, P. Boolchand, A. Pradel, J. Chem. Phys. **143**, 074502 (2015).
[79] S. Raoux, W. Welnic, D. Ielmini, Chem. Rev. **110**, 240 (2010).
[80] Raty Nature Comm ou Fons et Kolobov
[81] M. Bauchy, M. Micoulaut, M. Boero, C. Massobrio, Phys. Rev. Lett. **110**, 165501 (2013).
[82] S. Le Roux and P. Jund, Comput. Mater. Sci. **50**, 1217 (2011).
[83] V. King, Nature (London) **213**, 1112 (1967).
[84] D. S. Franzblau, Phys. Rev. B **44**, 4925 (1991).
[85] S. Le Roux, A. Bouzid, M. Boero, C. Massobrio, Phys. Rev. B **86**, 224201 (2012).
[86] X. Yuan, A.N. Cormack, Comp. Mater. Sci. **24**, 343 (2002).
[87] M. Micoulaut, X. Yuan, L.W. Hobbs, J. Non-Cryst. Solids **353**, 1951 (2007).
[88] F.H. Stillinger, T.A. Weber, R.A. La Violette, J. Chem. Phys. **85**, 6460 (1986).
[89] P.M. Bridenbaugh, G.P. Espinosa, J.E. Griffiths, J.C. Phillips, J.P. Remeika, Phys. Rev. B **20**, 4140 (1979).
[90] P.K. Gupta, J.C. Mauro, J. Chem. Phys. **126**, 224504 (2007).
[91] J.C. Mauro, P.K. Gupta, R.J. Loucks, J. Chem. Phys. **130**, 234503 (2009).
[92] F. J. Bermejo, C. Cabrillo, E. Bychkov, P. Fouquet, G. Ehlers, W. Häussler, D. L. Price, and M. L. Saboungi, Phys. Rev. Lett. **100**, 245902 (2008).
[93] E. L. Gjersing, S. Sen, and R. E. Youngman, Phys. Rev. B**82**, 014203 (2010).